

Gap Anisotropy in Iron-Based Superconductors: A Point-Contact Andreev Reflection Study of $\text{BaFe}_{2-x}\text{Ni}_x\text{As}_2$ Single Crystals

Cong Ren^{1,†}, Zhao-Sheng Wang¹, Zhen-Yu Wang¹, Hui-Qian Luo¹, Xing-Ye Lu¹,

Bin Sheng¹, Chun-Hong Li¹, Lei Shan¹, Huan Yang^{1,2}, and Hai-Hu Wen^{1,2}

¹ National Laboratory for Superconductivity, Institute of Physics
and Beijing National Laboratory for Condensed Matter Physics,

Chinese Academy of Sciences, P.O. Box 603, Beijing 100190, China and

² Physics Department, Nanjing University, Nanjing 210093, Jiangsu, China

We report a systematic investigation on c -axis point-contact Andreev reflection (PCAR) in $\text{BaFe}_{2-x}\text{Ni}_x\text{As}_2$ superconducting single crystals from underdoped to overdoped regions ($0.075 \leq x \leq 0.15$). At optimal doping ($x = 0.1$) the PCAR spectrum feature the structures of two superconducting gap and electron-boson coupling mode. In the s_{\pm} scenario, quantitative analysis using a generalized Blonder-Tinkham-Klapwijk (BTK) formalism with two gaps: one isotropic and another angle dependent, suggest a nodeless state in strong-coupling limit with gap minima on the Fermi surfaces. Upon crossing above the optimal doping ($x > 0.1$), the PCAR spectrum show an in-gap sharp narrow peak at low bias, in contrast to the case of underdoped samples ($x < 0.1$), signaling the onset of deepened gap minima or nodes in the superconducting gap. This result provides evidence of the modulation of the gap amplitude with doping concentration, consistent with the calculations for the orbital dependent pair interaction mediated by the antiferromagnetic spin fluctuations.

PACS numbers: 74.20.Rp, 74.25.Ha, 74.70.Dd

It is generally accepted that superconductivity in iron pnictides results from a superexchange repulsion mediated by magnetic excitations, which couple electron and hole pockets of the Fermi surface [1–3]. Such pairing interactions favor either isotropic s -wave order parameters with opposite signs on different sheets of the Fermi surface (FS) (s_{\pm} model) or anisotropic s -wave or even d -wave order parameters with nodes [4, 5]. Consensus has been reached on several systems, e. g. LaFePO [6], KFe_2As_2 [7], $\text{BaFe}_2(\text{As}_{1-x}\text{P}_x)_2$ [8], and so on, that nodes exist on the gap structure. However, experimental confirmations of such a nodal-gap state remains highly controversial in other systems [9–20]. For example, measurements of the electronic specific heat of $\text{Ba}(\text{Fe}_{1-x}\text{Co}_x)_2\text{As}_2$ have shown a field dependence consistent with both a fully gapped FS [12] and a nodal quasiparticles at the Fermi level [16, 17]. Such scattered experimental results and interpretations may come from the different qualities and doping level of the samples studied.

Point-contact Andreev reflection (PCAR) spectroscopy has been adopted for probing the density of state (DOS) of superconductors with the high energy resolution. In addition, the capability of this technique to study the anisotropy and the temperature dependence of the superconducting gap make it a unique tool in providing invaluable information for various mechanisms of unconventional superconductivity (for a review, see Refs. 21, 22). Several theoretical calculations have been reported on the PCAR conductance characteristics of a junction involving the s_{\pm} symmetry in iron pnictide superconductors [23, 24]. However, due to the long-standing issue of surface or/and interface degradation,

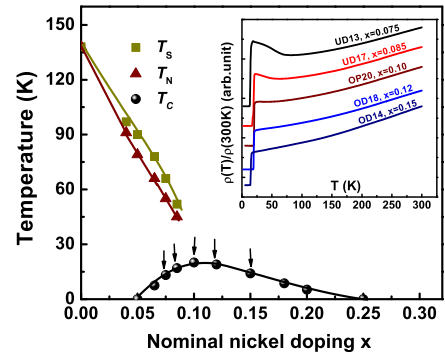


FIG. 1: (Color online) Phase diagram of $\text{BaFe}_{2-x}\text{Ni}_x\text{As}_2$ as a function of Ni concentration x . The orthorhombic phase below T_s and the antiferromagnetic (AF) phase below T_N are also shown here. The arrows indicate the doping levels of the samples under investigation. Inset: Temperature dependence of the in-plane resistivity ρ for samples with the Ni nominal doping level x as labeled. Data are vertically shifted for clarity.

experimental results by PCAR technique reveal a wide variation in the measured Andreev conductance spectra and consequently, the gap values, especially for the case of c -axis junctions [25, 26]. In this Letter, we fabricate highly transparent c -axis direct contacts to perform the PCAR spectroscopy study on a series of electron-doped $\text{BaFe}_{2-x}\text{Ni}_x\text{As}_2$ single crystals over a wide doping range. The conductance spectra show a systematic and consistent behavior with the variation of the doping level, indicative of a doping dependence of the order parameter for Ni-122 superconductor. In the s_{\pm} scenario, by using a generalized two-gap Blonder-Tinkham-Klapwijk (BTK)

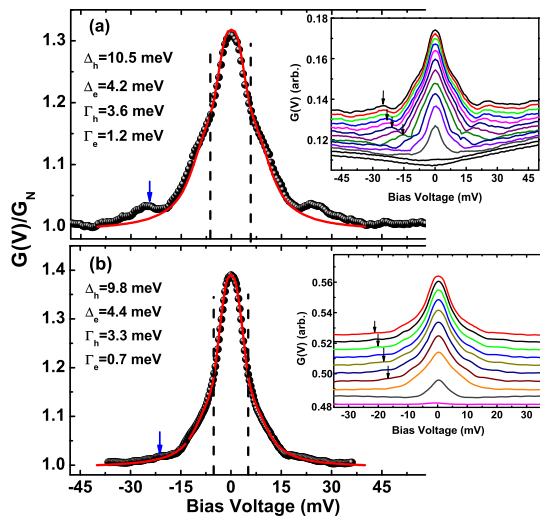


FIG. 2: Normalized conductance curves at $T = 2$ K for c -axis contacts (a) OP20a and (b) OP20b. The red solid lines are their two-gap fits with the relevant fitting parameters. The blue arrows indicate the additional conductance peak at the edge of gap and the dashed lines mark the “kink” structures in the main-gap $G(V)$ curves. Insets: the raw $G(V)$ curves in temperatures from 2 K to 21 K in a step of 2 K. Data are vertically shifted for clarity. The black arrows mark the corresponding edge-gap conductance peaks in the raw $G(V)$ curves for OP20a and OP20b, respectively.

model, we estimate the gap amplitude on the hole and electron FS sheets.

High-quality single crystals of $\text{BaFe}_{2-x}\text{Ni}_x\text{As}_2$ were grown from a self-flux method, as described elsewhere [27]. The crystals were characterized using x-ray diffraction and energy dispersion (EDX). The doping level in the crystals was determined by inductive coupled plasma emission spectrometer (ICP), which gave a Ni concentration roughly 0.8 times the nominal content x . We choose five compositions: underdoped, $x=0.075$ (UD13), 0.085 (UD17); overdoped, with $x=0.12$ (OD18), 0.15 (OD14), and optimally doped with $x = 0.1$ (OP20). The typical level of impurity phases has been checked by specific heat measurement on the optimally doped crystal $x = 0.1$, in which a residual component γ_0 at $T \rightarrow 0$ revealed an impurity phases of $\sim 4\%$ [28]. The temperature dependence of resistivity for these five compositions under investigation is displayed in inset of Fig. 1, by which the bulk transition temperature T_c is determined (95% of the normal state resistivity) for each composition. Consequently, the T_c value for each composition is shown on the phase diagram in the main panel of Fig. 1.

Point contacts to the flat and shiny surfaces cleaved along the c -axis of $\text{BaFe}_{2-x}\text{Ni}_x\text{As}_2$ crystals were made using thick silver paste (4929N DuPont) bonding with gold wires (of 16 μm diameter). The typical size of these planar contact is about 0.08-0.15 mm under a microscope. Due to the nanocrystalline nature of the silver paint, the

contact made in this way, is actually formed by many nanocontacts analog to tip point-contact technique [22]. For the backside electrical wiring, we applied ultrapure indium or silver paste to cover the whole area of the bottom surfaces of the crystals. On each piece of the crystal, 5-6 planar contacts were made from point to point to ensure the reproducibility and consistency of the junction conductance spectra and their spectroscopic nature.

Fig. 2(a) and (b) show the raw (inset) and normalized conductance curves $G(V) = dI(V)/dV$ of two c -axis $\text{Ag}/\text{BaFe}_{1.9}\text{Ni}_{0.1}\text{As}_2$ point contacts (OP20a and OP20b), respectively. The contacts made in this way remain stable in thermal cycling, and the contact resistance at high bias R_N varies very little ($< 6\%$) over the whole T range up to T_c . The Andreev signal as the conductance enhancement decreases on increasing T and vanishes at $T \geq T_c$, leaving a slightly asymmetrical V -shaped normal state. Shown in the main panels of Fig. 2(a) and (b), the magnitude of the Andreev reflection reaches as high as 30%-40%, implying a relatively transparent boundary between Ag nanoparticle and $\text{BaFe}_{2-x}\text{Ni}_x\text{As}_2$ superconductors. The stabilities in R_N and the high level of Andreev signal indicate that the conduction channels through the contact is in ballistic regime, and therefore, energy-resolved spectroscopy is possible. A feature shows up in these conductance curves: an additional peak at ~ 20 mV, and the peak gradually disappears with T approaching T_c . It seems that this peak is much pronounced when the Andreev signal is relatively low, which is close to the case of tunneling side (see below). Very recently, this conductance peak at the edge of the gap has been observed in Co-122 crystals [29], and is attributed to the signature of an electron-boson coupling associated with the superconducting gap. The observation of the electron-boson coupling mode in the conductance spectra implies the high quality of the point-contacts and thus their spectroscopic nature.

The two-gap superconductivity manifests itself as a “kink” in the in-gap conductance, marked at the dashed lines in Fig. 2 (a) and (b). To explicitly describe the variety of spectral behavior observed and quantitatively resolve the gap amplitude, we invoke a generalized BTK formula [30] with three parameters: a dimensionless parameter Z which represents the interface transparency; an imaginary quasiparticle energy modification Γ [31] which reflects the spectral broadening, and the superconducting gap Δ . In BTK model, the normal and Andreev reflection probabilities, respectively, are related to the DOS of the superconductor $N_s = N_0 \text{Re}(\frac{E-i\Gamma}{\sqrt{(E-i\Gamma)^2 - \Delta^2(T,\theta)}})$ with N_0 the normal-state DOS and θ the crystalline angle parallel to the current injection. To choose a gap function to calculate these two-gap conductance spectra, we assume, based on the s_{\pm} scenario, an isotropic gap Δ_h and an anisotropic gap of the general form $\Delta_e[1 - r + r \cos(2\theta)]$, with the gap

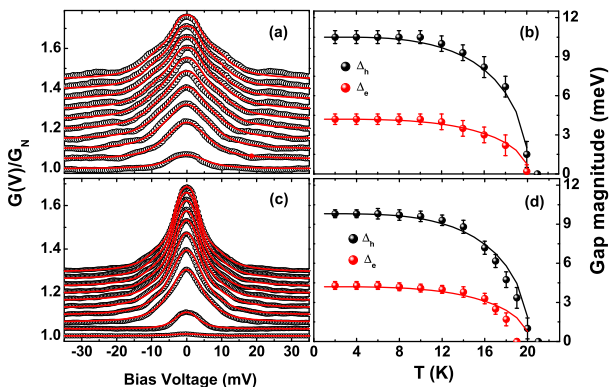


FIG. 3: (Color online) Temperature dependence of the normalized conductance spectra and the relevant two-gap BTK fits (solid red lines) for (a) OP20a, and (b) OP20b, respectively. Data and their fits are vertically shifted for clarity except the bottom ones. The step of T increase is 2 K. The obtained gap magnitude for (b) OP20a, and (d) OP20b, respectively, as a function of T . The solid lines are the fits to an empirical gap function, see text.

anisotropy ratio r varying from $r = 0$ (isotropic s_{\pm} state) to $r = 1$ (completely d -wave) [20, 32, 33]. Therefore, by the standard two component conductance (current) model the conductance spectra is the contributions of the hole-like (G_h) and electron-like (G_e) Fermi pockets: $G = wG_h + (1 - w)G_e$, where w is the spectral weight. For simplicity, we assume a balanced contribution of hole and electron Fermi surfaces to the spectral conductance by taking $w=0.5$.

Examples of normalized $G(V)$ curves and their fits at $T = 2$ K are shown in the main panels of Fig. 2(a) and (b) for junctions OP20a and OP20b, respectively. The two-gap BTK model (red lines) fit very well the main features of the experimental $G(V)$ curves except the electron-boson coupling mode around 20 meV, yielding a set of fitting parameters associated with gap magnitude and anisotropy ratio: $\Delta_h = 10.5$ meV, $\Delta_e = 4.2$, and $r = 0.3$ for OP20a and $\Delta_h = 9.5$ meV, $\Delta_e = 4.5$ meV, and $r = 0.3$ for OP20b, respectively. It is noted that the same gap magnitude is also extracted from a recent PCAR experiment on a c -axis Ag/BaFe_{1.8}Co_{0.2}As₂ with the comparable $T_c = 24$ K [29]. Here we emphasize that a two-gap formula with two s -wave gap ($r = 0$) can also fits our experimental data rather well. However, the parameters $\Gamma/\Delta = 0.6 - 0.7$ are applied to fulfill the fit at this low T , which brings a large uncertainty in the gap magnitude.

With these fitting parameters, we check the validity of these fits by extending the fit to the overall temperature spectral. As shown in Fig. 3(a) and (c), the two-gap s_{\pm} model still fits reasonably well the T -dependence of these $G(V)$ curves with fitted gap magnitude. In this overall- T spectral fit, $r = 0.3$ and $Z_{h(e)} = 0.3 - 0.2$ are constant with T while $\Gamma_h = 3.3$ and $\Gamma_e = 1.3$ meV (OP20a)

and $\Gamma_h = 2.9$ and $\Gamma_e = 0.8$ meV (OP20b) are almost constant or slightly increase with T . From the fits of various curves we obtain the gaps Δ_h and Δ_e as a function of T , which is plotted in Fig. 3(b) and (d) for these two junctions, respectively. For comparison, the obtained gaps can be approximated by an empirical gap formula: $\Delta(T) = \Delta_0 \tanh(\alpha\sqrt{T_c/T - 1})$ with $\alpha = 1.95$ for Δ_h and 1.86 for Δ_e (cf. $\alpha = 1.74$ for weak-coupling BCS gap).

We analyze the physical meanings of the obtained gap values and gap function. It is shown from angle-resolved photoemission spectroscopy experiment on a Co-122 crystal that the large gap Δ_h is located on one of the electron FS sheets, instead, the small gap Δ_e is presented on one of the hole FS sheets [10]. The gap values $2\Delta_h/k_B T_c \approx 11.6$ and $2\Delta_e/k_B T_c \approx 5.0$, both above the BCS weak-coupling ratio. Besides, the α value from the $\Delta(T)$ function also points to a strong-coupling character for both Δ_h (hole FS) and Δ_e (outer electron FS). These results are consistent with a three-band s_{\pm} Eliashberg model [34], in which spin fluctuations mainly provide the interband coupling, and thus so in the electron-boson coupling matrix. On the other aspect, the existence of strong electron-boson coupling in this compound is manifested by the observation of the spectral peak E_p at about 20 meV. In our low-transparency (large $Z = 0.3$ for OP20a) point contact, a characteristic energy of $\Omega_b = E_p - \Delta_{max} = 13$ meV and 11 meV (OP20b junction with small $Z = 0.2$). This energy scale is compatible with the spin-resonance energy observed by neutron scattering on the same crystals [35].

The obtained anisotropy ratio $r = 0.3$, resolved in our c -axis PCAR spectroscopy of BaFe_{1.9}Ni_{0.1}As₂, indicates a full gap state with gap minima along c axis. This nodeless state of optimally doped Ni-122 is in similarity with that of optimally-doped Co-122, in which a gap minima is already present at maximal T_c by the c -axis thermal conductivity measurements [13, 36].

It is natural, however, to inspect the manner of the superconducting gaps in the crystals with doping away from the optimum. We have measured the point-contact $G(V)$ curves in whole T range up to T_c for junctions with $x = 0.075$ (UD13), 0.085 (UD17), 0.12 (OD18), and 0.15 (OD14). The typical $G(V)$ curves at $T = 2$ K ($< 0.2 T_c$) and $T \geq T_c$ are shown in Fig. 2(a)-(d) for these four samples respectively. As shown, these $G(V)$ curves exhibit a consistent behavior: 1) An underlying feature of a *dominant* single gap is unambiguously identified with a similar conductance enhancement of 25%-35% for each junction; 2) A parabolic normal-state $G(V)$ curve with a slight asymmetry at $T \geq T_c$ for each x , opposite to those of hole-doped K-122 [11, 26], implies the similar origin of the underlying normal-state background. Nevertheless, a striking feature in these normalized (and the raw) $G(V)$ curves is that: at $T = 2$ K, a conductance plateau and/or a double peak around zero bias for junctions UD13 and UD17 gradually evolves into an in-gap

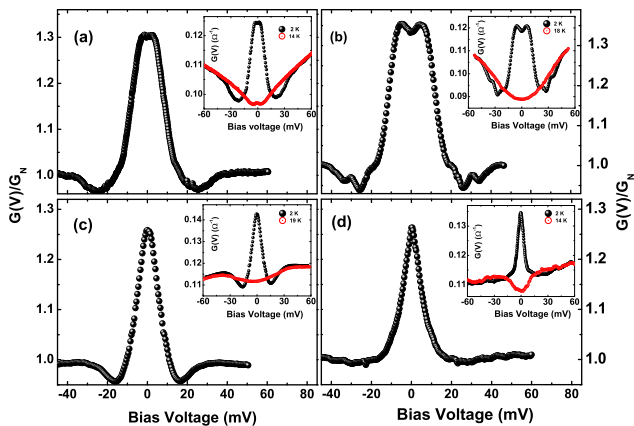


FIG. 4: Normalized conductance curves at $T = 2\text{K}$ for (a) UD13, (b) UD17, (c) OD18, and (d) OD14. Insets: The corresponding raw data of conductance spectra at 2K and $T \geq T_c$.

sharp peak in $G(V)$ for junctions OD18 and OD14. Considering the overall spectral consistency in these junctions, the systematic evolution of the Andreev conductance spectra with doping concentration is nontrivial. Qualitatively, for highly transparent junctions at finite T , the appearance of an in-gap plateau in Andreev conductance spectrum is a signature of a fully gapped state. In contrast, an in-gap conductance peak is a characteristic of an anisotropic gap state due to the presence of a finite DOS at low energy, like a d -wave gap in cuprates [21]. We note that it is not easy to describe the spectral behavior using simple formalism, because we are dealing with multi-band or/and even multi-gap system. Therefore, our observation that the systematic evolution from the in-gap conductance plateau for the underdoped samples to the in-gap peak in $G(V)$ curves for the overdoped samples indicates the existence of doping induced evolution of superconducting gaps with an isotropic feature in the underdoped region to an anisotropic, even, nodal gap in the overdoped side. This is highly consistent with the result of the T -dependent penetration depth λ in a series of Ni-122 superconductors, in which $\Delta\lambda \propto T^n$ with the exponent $n \geq 2$ for underdoped samples and $\Delta\lambda$ becomes more linear- T dependent for overdoped samples, indicating the development of nodal gaps in the overdoped region [14].

In conclusion, measurements on point-contact junctions made on single crystals of $\text{BaFe}_x\text{Ni}_{1-x}\text{As}_2$ illustrate an interesting evolution of the gap structure. The Andreev conductance spectra clearly show a full-gap state for underdoped crystals and a highly anisotropic, perhaps nodal-like gap state for overdoped crystals. Quantitative analysis of the spectral data of optimally-doped contacts using a generalized BTK formalism resolves two superconducting gaps in strong coupling limit. Resulted

from the analytical fitting, the small gap on the electron-like FS sheets shows a crossover from a nodeless in the underdoped side to a nodal feature in the overdoped region. This result provides evidence of the modulation of the gap amplitude on the FS with doping concentration, consistent with the calculation for the orbital dependent pair interaction mediated by the antiferromagnetic spin fluctuations.

Acknowledgement: The authors are grateful to Profs. R. Prozorov, Qiang-Hua Wang and Dr. Gang Mu for intensive discussions. This work is supported by the National Science Foundation of China, the Ministry of Science and Technology of China (973 project No: 2011CBA00100), and Chinese Academy of Sciences (Project ITSNEM).

†cong.ren@iphy.ac.cn

-
- [1] I. I. Mazin *et al.*, *Phys. Rev. Lett.* **101**, 057003 (2009).
 - [2] F. Wang *et al.*, *Phys. Rev. Lett.* **102**, 047005 (2008).
 - [3] K. Kuroki *et al.*, *Phys. Rev. Lett.* **101**, 087004 (2008).
 - [4] K. Kuroki *et al.*, *Phys. Rev. B* **79**, 224511 (2009).
 - [5] S. Graser *et al.*, *Phys. Rev. B* **81**, 214503 (2010); T. A. Maier, *et al.*, *Phys. Rev. B* **79**, 224510 (2009).
 - [6] D. Fletcher *et al.*, *Phys. Rev. Lett.* **102**, 147001 (2009); C. W. Hick *et al.*, *Phys. Rev. Lett.* **103**, 127003 (2009).
 - [7] J. K. Dong *et al.*, *Phys. Rev. Lett.* **104**, 087005 (2009); K. Hashimoto *et al.*, *Phys. Rev. B* **82**, 014526 (2010).
 - [8] K. Hashimoto *et al.*, *Phys. Rev. B* **81**, 220501 (2010).
 - [9] H. Ding *et al.*, *EPL*, **83**, 47001 (2008).
 - [10] K. Terashima *et al.*, *Proc. Natl. Acad. Sci. U.S.A.* **106**, 7330 (2009).
 - [11] X. H. Zhang *et al.*, *Phys. Rev. Lett.* **102**, 147002 (2009); *ibid.* *Phys. Rev. B* **82**, 020515(R) (2010).
 - [12] F. Hardy *et al.*, *Phys. Rev. Lett.* **102**, 187004 (2009); *ibid.*, *arXiv:1007.2218*.
 - [13] J.-Ph Reid *et al.*, *Phys. Rev. B* **82**, 064501 (2010).
 - [14] R. Prozorov *et al.*, *Phys. Rev. B* **80**, 174517 (2009).
 - [15] C. Martin *et al.*, *Phys. Rev. B* **81**, 060505 (2010).
 - [16] K. Gofryk *et al.*, *Phys. Rev. B* **83**, 064513 (2011).
 - [17] G. Mu *et al.*, *arXiv: 1103.1300* (2011).
 - [18] H. Fukazawa *et al.*, *J. Phys. Soc. Jpn* **78**, 033704 (2009).
 - [19] B. Muschler *et al.*, *Phys. Rev. B* **80**, 180510(R) (2009).
 - [20] E. Schachinger, and J. P. Carbotte, *Phys. Rev. B* **80**, 174526 (2009); D. Wu, *et al.*, *Phys. Rev. B* **82**, 184527 (2010).
 - [21] G. Deutscher, *Rev. Mod. Phys.* **77**, 109 (2005)
 - [22] D. Daghero, and R.S. Gonnelli, *Supercond. Sci. Technol.* **23**, 043001 (2010).
 - [23] A. A. Golubov *et al.*, *Phys. Rev. Lett.* **103**, 077003 (2009); P. Ghaemi, F. Wang, and A. Vishwanath, *Phys. Rev. Lett.* **102**, 157002 (2009).
 - [24] Da Wang, Yuan Wan, and Qian-Hua Wang, *Phys. Rev. Lett.* **102**, 197004 (2009); I. B. Sperstad, J. Linder, and A. Sudbø, *Phys. Rev. B* **80**, 144507 (2009). M. A. N. Araujo and P. D. Sacramento, *Phys. Rev. B* **79**, 174529 (2009).
 - [25] P. Samuely *et al.*, *Physica C* **469**, 507 (2009).
 - [26] Xin Lu *et al.*, *Supercond. Sci. Technol.* **23**, 054009 (2009).

- [27] Yan-Chao Chen *et al.*, *SST* **24**, 065004 (2011).
- [28] Bing Zeng *et al.*, *arXiv*:1006.2785.
- [29] M. Tortello *et al.*, *Phys. Rev. Lett.* **105**, 237002 (2010).
- [30] G. E. Blonder, M. Tinkham, and T. M. Klapwijk, *Phys. Rev. B* **25**, 4515 (1982).
- [31] R. Dynes *et al.*, *Phys. Rev. Lett.* **41**, 1509 (1978).
- [32] A. V. Chubukov, M. G. Vavilov, and A. B. Vorontsov, *Phys. Rev. B* **80**, 140515(R) (2009).
- [33] A. B. Vorontsov, and I. Vekhter, *Phys. Rev. Lett.* **105**, 187004 (2010); I. I. Mazin, *et al.*, *Phys. Rev. B* **82**, 180502 (2010).
- [34] G. A. Ummarino *et al.*, *Phys. Rev. B* **80**, 172503 (2009); L. Benfatto, E. Cappelluti, and C. Castellani, *Phys. Rev. B* **80**, 214522 (2009).
- [35] Miaoyin Wang *et al.*, *Phys. Rev. B* **81**, 174524 (2010).
- [36] M. A. Tanatar *et al.*, *Phys. Rev. Lett.* **104**, 067002 (2010).